

## Coverage-Dependent Molecular Ejection from Ion-Bombarded C<sub>6</sub>H<sub>6</sub>/Ag{111}

R. Chatterjee, D. E. Riederer,<sup>†</sup> Z. Postawa,<sup>‡</sup> and N. Winograd\*

Department of Chemistry, The Pennsylvania State University, University Park, Pennsylvania 16802

Received: February 9, 1998; In Final Form: March 31, 1998

Time-of-flight distributions, angular distributions, and relative sputtering yields of neutral benzene (C<sub>6</sub>H<sub>6</sub>) molecules ejected from submonolayer to multilayer coverage of C<sub>6</sub>H<sub>6</sub> on Ag{111} have been measured after 8 keV ion bombardment. Two components are present in the time-of-flight distributions obtained using Ar<sup>+</sup> ion as the projectile. For low coverage a peak corresponding to kinetic energies ranging between 0.25 and 1 eV dominates the distribution, whereas for multilayer coverage a peak corresponding to extremely low kinetic energy (0.04 eV) becomes dominant. The total yield of the ejected neutral C<sub>6</sub>H<sub>6</sub> molecules is largest for a monolayer coverage and decreases to ~50% of the maximum for multilayer samples. For low coverage, the C<sub>6</sub>H<sub>6</sub> kinetic energy and angular distributions take on the same characteristics as that of silver particles ejecting from the substrate, indicating that collisions originating in the metal substrate lead to the ejection of C<sub>6</sub>H<sub>6</sub> molecules. The low kinetic energy emission of molecules from the multilayer films is proposed to occur due to exothermic chemical reaction of fragments formed in a molecular collision cascade initiated by the projectile ions. Finally, for the entire coverage range investigated, no C<sub>6</sub>H<sub>6</sub> signal is observed when H<sub>2</sub><sup>+</sup> ion is used as the projectile, indicating that a momentum-transfer process is important in the ejection of C<sub>6</sub>H<sub>6</sub> molecules.

### Introduction

The elucidation of the mechanism of ion-beam-induced desorption of organic molecules from surfaces is of current interest.<sup>1–4</sup> Knowledge of these mechanisms is needed not only to optimize a variety of molecular surface analysis experiments but also to provide complementary information that might be helpful in understanding the behavior of other stimulated-desorption probes such as those involving electron beams and laser beams. Molecular desorption itself is an intriguing phenomenon since intact molecules can be ejected by a projectile that possesses many orders of magnitude more energy than is contained in most chemical bonds.

There are a range of possible mechanisms that have been put forth to describe the ejection of organic molecules.<sup>5–10</sup> These involve sputtering via a collision cascade and momentum transfer,<sup>11–14</sup> various thermal desorption mechanisms,<sup>15,16</sup> and even mechanisms involving electronic processes.<sup>17,18</sup> The type of mechanism proposed is generally determined by the behavior of the velocity or kinetic energy distribution of the emitted molecules. Collision cascade-induced desorption is thought to follow a Thompson-like distribution<sup>19</sup> while thermal emission is often invoked when the distributions are similar to a Maxwell–Boltzmann distribution. Velocity distributions of electron-stimulated desorbed species are narrow and are peaked at energies that depend on the electronic structure of the adsorbate.<sup>20</sup>

It is important to be able to isolate the contributions of the various mechanisms that lead to molecular ejection. If momentum transfer between the primary ion and the target is the

most important process, then the ejection must occur in a nonequilibrium fashion and can, in principle, be described using molecular dynamics computer simulations. If there is a thermal component, then the energy of the primary ion must be converted into heat. Mechanisms involving electronic excitation are unique in that emission should occur even with bombardment by electrons or light ions such as H<sub>2</sub><sup>+</sup>.

There is not a long history of well-defined measurements that spotlight the important mechanisms. Most studies have been performed on ejected ions rather than neutral molecules. Interpretation of ion data is complicated since the nuclear motion is convoluted with the ionization process. Several studies have carefully examined the behavior of molecules ejected from frozen gases.<sup>17,18,21,22</sup> These studies are also problematic from a mechanistic viewpoint since the experiments are performed using a high dose of incident ions. In these cases, multiple ion impacts may over time impart enough heat to the target to allow simple evaporation. In addition, there can be an accumulation of damage that alters the chemical composition of the target.

Distinction between the various mechanisms is not a simple matter for molecular systems. For collision cascades in atomic solids, for example, the Thompson distribution is often useful.<sup>19</sup> This distribution describes the yield of the ejected species as a function of the kinetic energy. It exhibits a maximum yield for  $E = E_b/2$ , where  $E_b$  is the surface binding energy of the bombarded material and shows an  $E^{-2}$  dependence for  $E \gg E_b$ . The model is rigorously applicable to bombarded amorphous targets where the collision cascade is fully developed but may not be appropriate for atomic or molecular adsorbates<sup>23</sup> where the cascade is only partially developed.<sup>24</sup> Another complication relevant to molecular ejection involves the fact that molecules that eject as a result of high-energy collisions often experience fragmentation. Selective depletion of these internally hot molecules in fact distorts the resulting kinetic energy distribution. Few models have been proposed to account for this

\* To whom correspondence should be addressed.

<sup>†</sup> Permanent address: Department of Chemistry, University of Missouri, Columbia, MO 65211.

<sup>‡</sup> Permanent address: Institute of Physics, Jagellonian University, ul. Reymonta 4, PL-30059, Krakow 16, Poland.

phenomenon.<sup>25</sup> These models predict that the kinetic energy distribution of ejected molecules falls as  $E^{-2}$  at kinetic energies higher than the surface binding energy but lower than the dissociation energy of the molecule. At kinetic energies much larger than the dissociation energy of the molecule, the distribution is described by  $E^{-n}$  where the value of  $n$  depends on the model. Similar complications arise with processes that appear to exhibit thermal character. For Maxwell–Boltzmann distributions, for example, the fit temperature is generally much different than the substrate temperature, and its value may have no physical meaning. It has, therefore, neither been possible to establish the fundamental principles associated with molecular desorption nor establish a general theoretical framework for understanding the experimental results.

In the present study, time-of-flight (TOF) and angular distributions of the ejected neutral benzene (C<sub>6</sub>H<sub>6</sub>) molecules after kiloelectronvolt ion bombardment of C<sub>6</sub>H<sub>6</sub> adsorbed on Ag{111} are reported. The experiments are unique in that the measurements are performed using sufficiently low incidence ion doses such that there is no observable surface modification. Hence, the translational energies, ejection angles, and relative yields obtained from these measurements provide fundamental information about the molecular ejection process.

Benzene/Ag{111} has been used as a model system because Ag is fairly unreactive, and adsorption and desorption of C<sub>6</sub>H<sub>6</sub> on Ag{111} is reversible with temperature.<sup>26</sup> Moreover, the C<sub>6</sub>H<sub>6</sub> exposure can be varied systematically to obtain submonolayer to multilayer coverage, and thereby the role of the local molecular environment in the ejection process can be probed. The results show that the ejection mechanism depends strongly on coverage. For example, when just a few C<sub>6</sub>H<sub>6</sub> molecules are present on the Ag surface, the energy and angular distributions take on some of the characteristics of the distribution of the metal substrate. The C<sub>6</sub>H<sub>6</sub> molecules in this case eject with kinetic energies close to 1 eV. As the coverage is increased, however, the kinetic energy distributions shift to lower energies peaking at 0.25 eV, due to collisions between the molecules. And finally, for multilayers of C<sub>6</sub>H<sub>6</sub>, the desorption behavior changes dramatically again, with the kinetic energy distribution peaking at 0.04 eV and exhibiting characteristics of a Maxwell–Boltzmann distribution. To our knowledge this is the first set of coverage-dependent data clearly showing how increase in molecular coverage affects the kinetic energy distributions.

## Experimental Section

The apparatus used to measure energy- and angle-resolved neutral (EARN) distributions is described in detail elsewhere.<sup>27</sup> Briefly, the measurements were performed in an ultrahigh-vacuum chamber ( $1.5 \times 10^{-10}$  Torr base pressure) equipped with low-energy electron diffraction (LEED) and Auger electron spectroscopy (AES) for surface characterization. A desorption event was initiated by a 220 ns pulse of 8 keV projectile ions focused to a 3 mm diameter spot on the surface. Soon after ion impact, an electric field was applied to a grid in front of the sample to prevent the secondary ions ejected from the surface from reaching the laser plane. The ejected neutral species were detected by nonresonant two-photon ionization using 6 ns laser pulses at 266 nm obtained from a frequency-quadrupled Nd:YAG laser operated at a repetition rate of 30 Hz. The laser beam was focused to a ribbon shape (1 mm  $\times$  10 mm cross section) and was positioned approximately 1 cm above the sample. Accurate surface to laser distance measurements were made using a telescope mounted on a micrometer before each experiment.

The ionized particles were accelerated toward a position-sensitive microchannel plate (MCP) detector. The image was displayed on a phosphor screen and monitored by a charge-couple-device camera interfaced to a Pentium PC computer for data storage and processing. The MCP detector voltage was pulsed for mass selection. A mass resolution of approximately 20 at  $m/z$  100 was obtained by this method. The time-of-flight (TOF) distributions of the neutral molecules were recorded by varying the delay between the ion pulse and the laser pulse. Energy distributions were obtained after coordinate transformation of the measured TOF distributions.<sup>27</sup> The angle of incidence of the primary ion beam was 45°, and the desorbed neutral molecules were detected normal to the surface within an angular range of  $\pm 20^\circ$  during the TOF measurements. The energy-integrated angular distribution measurements were made with a 0° incident projectile. The distributions were obtained after averaging 100 laser shots at each delay time. The measurements were made under static conditions, and the primary ion dose was kept below  $10^{12}$  ions/cm<sup>2</sup> in all experiments.

The Ag{111} crystal was cleaned with alternate cycles of sputtering and annealing at 450 °C until sharp LEED spots were obtained. Benzene vapor was introduced into the chamber using a leak valve and was condensed onto a clean Ag{111} crystal cooled to 120 K. The gases dissolved in C<sub>6</sub>H<sub>6</sub> were removed by several freeze–pump–thaw cycles before dosing. All exposures are reported in langmuir units (1 langmuir =  $1 \times 10^{-6}$  Torr·s) and are uncorrected for the ion gauge sensitivity factor of 5.8.<sup>28</sup> Various exposures of C<sub>6</sub>H<sub>6</sub> ranging from 0.3 to 800 langmuirs were investigated. We were unable to observe the (3  $\times$  3) LEED pattern at 5 langmuirs C<sub>6</sub>H<sub>6</sub> exposure as previously reported.<sup>29,30</sup> Our LEED apparatus is not sensitive enough to allow study of ordered overlayers since electron beam damage occurs rapidly at the flux required to see diffraction spots.

Surface charging by the primary ion is of concern in nonconducting solids because it causes instability in the signal and in extreme cases deflection of the primary ion away from the sample. We do not believe that charging effects are influencing our results in any way. First, our experiments are performed at low primary ion doses that produce minimal charge accumulation. Second, the thickness of the investigated overlayers is small ( $\leq 0.07 \mu\text{m}$ ), allowing the extra charge to dissipate into the metal substrate. Third, the signal intensity is always stable and reproducible over the course of the measurements. And finally, flooding the surface with low-energy electrons does not affect the intensity of the measured signal.

The mass spectrum of the ejected particles nonresonantly ionized by the laser is shown in Figure 1. The spectrum exhibits prominent peaks at  $m/z$  52 (C<sub>4</sub>H<sub>4</sub> fragment), 78 (C<sub>6</sub>H<sub>6</sub>), 108 (Ag), and 216 (Ag<sub>2</sub>). However, the possibilities that other particles were ejected but were either not ionized or were fragmented by the laser cannot be excluded. The mass spectrum obtained from multiphoton ionization of gaseous C<sub>6</sub>H<sub>6</sub> also exhibits peaks at  $m/z$  78 and 52, which are nearly identical to those observed in the mass spectrum of the sputtered particles. The relative contribution of fragments and molecular species depends on the laser power. At a lower laser power (0.8 mJ/pulse) the C<sub>4</sub>H<sub>4</sub> signal is entirely eliminated. This observation indicates that all the molecules constituting the peak at  $m/z$  52 originates from photofragmentation of C<sub>6</sub>H<sub>6</sub>. This conclusion is further confirmed by the fact that the TOF distributions of measured C<sub>4</sub>H<sub>4</sub> and C<sub>6</sub>H<sub>6</sub> are identical. Regardless of the significant sensitivity of the mass spectrum to the laser power,

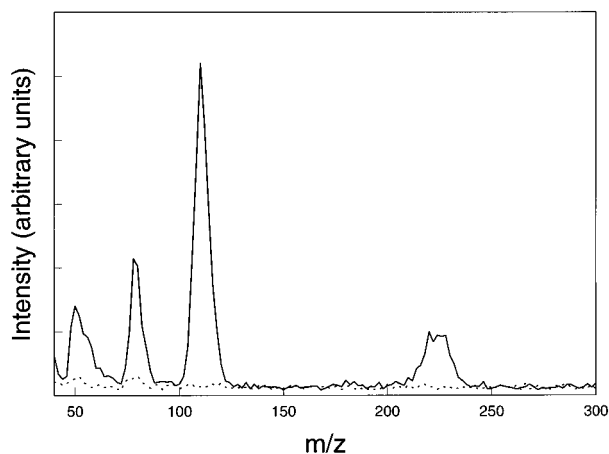


**Figure 1.** Multiphoton ionization mass spectra using a focused 266 nm laser beam (3 mJ/pulse). The spectrum displays the laser-ionized neutral molecules ejected after 8 keV Ar<sup>+</sup> ion bombardment (solid line) and the background obtained in the absence of the ion pulse (dotted line). The mass spectrum is for 100 langmuirs exposure (uncorrected for ion gauge sensitivity factor of 5.8).

the TOF distributions do not depend on this parameter for up to laser energies of 3 mJ/pulse. The distributions were therefore obtained at the higher laser power where a better signal-to-noise ratio could be achieved. For the ejected substrate particles, the distributions were recorded for Ag<sub>2</sub>. As in the case of C<sub>6</sub>H<sub>6</sub>, the Ag<sub>2</sub> TOF distributions do not vary with the degree of fragmentation within the investigated laser power range.

## Results and Discussion

**Coverage Dependence.** To unravel the various factors that may contribute to molecular ejection, we chose to examine ejection yields, kinetic energy, and angular distributions of C<sub>6</sub>H<sub>6</sub> molecules emitted from C<sub>6</sub>H<sub>6</sub>/Ag{111} as a function of the C<sub>6</sub>H<sub>6</sub> coverage. In this way, it is possible to systematically alter the molecular environment of C<sub>6</sub>H<sub>6</sub> molecules such that in the beginning they exist in near isolation on a metal surface, and eventually they are bound into a multilayer of frozen C<sub>6</sub>H<sub>6</sub>. Under these conditions, it is also possible to examine the role of the metal substrate, the influence of intermolecular collisions, and the role of the changing chemical environment in affecting the ejection of a single type of molecule.

The total yields of ejected C<sub>6</sub>H<sub>6</sub> and Ag<sub>2</sub> molecules as a function of C<sub>6</sub>H<sub>6</sub> exposure are shown in Figure 2. The Ag<sub>2</sub> signal is largest for the clean surface and decreases with increasing C<sub>6</sub>H<sub>6</sub> exposure. The C<sub>6</sub>H<sub>6</sub> signal on the other hand initially increases with exposure. It reaches a maximum at 6 langmuirs and then drops to a constant value of ~50% of the maximum intensity for multilayer samples.

An estimate of the C<sub>6</sub>H<sub>6</sub> coverage can be obtained from this yield dependence. As mentioned earlier, at 5 langmuirs exposure, C<sub>6</sub>H<sub>6</sub> is known to form an ordered (3 × 3) overlayer on Ag{111} at 120 K.<sup>29,30</sup> It has also been reported that neutral and ion yields are largest for monolayer coverage of various organic molecules on metal substrates.<sup>6,31</sup> Hence, the occurrence of the maximum in the measured C<sub>6</sub>H<sub>6</sub> signal at 6 langmuirs exposure can be correlated with the formation of a complete monolayer. This conclusion is further supported by the following estimation. Assuming unit-sticking probability, the time required for monolayer formation is<sup>32</sup>

$$t = 4/(nvS)$$

where  $n$  is the gas-phase number density,  $v$  is the average

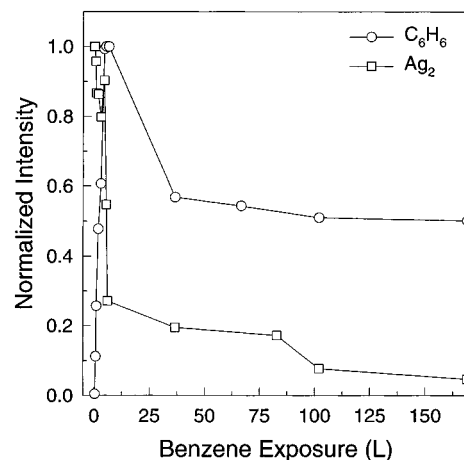


**Figure 2.** Normalized yields of C<sub>6</sub>H<sub>6</sub> and Ag<sub>2</sub> as a function of C<sub>6</sub>H<sub>6</sub> exposure in langmuirs. The exposures reported here and in Figures 3–9 are uncorrected for the ion gauge sensitivity factor of 5.8.

velocity, and  $S$  is the surface area per molecule. For room-temperature C<sub>6</sub>H<sub>6</sub> at  $1 \times 10^{-6}$  Torr,  $n = 3.2 \times 10^{16} \text{ m}^{-3}$ ,  $v = 71 \text{ m/s}$ , and  $S = 6.5 \times 10^{-19} \text{ m}^2$  (for  $3 \times 3$  C<sub>6</sub>H<sub>6</sub>/Ag{111}). From the above equation,  $t = 0.677 \text{ s}$ , which corresponds to an exposure of 0.7 langmuir. After incorporating the ion gauge sensitivity (5.8 for C<sub>6</sub>H<sub>6</sub>), the exposure required to form a monolayer would be 4 langmuirs, which compares reasonably with the experimentally obtained value of 6 langmuirs. Based on these calculations, 800 langmuirs exposure would correspond to ~130 layers.

The initial increase in the C<sub>6</sub>H<sub>6</sub> signal is expected as the coverage increases from a submonolayer value to a complete monolayer. The reason for the decrease in total yield above a monolayer coverage can be discerned from related observations. The effective mass of the subsurface species changes from being Ag at low coverage to being carbon-like at the highest exposures. In effect, the collision cascade is developed in the C<sub>6</sub>H<sub>6</sub> layers rather than in the Ag crystal. Molecular dynamics simulations investigating the effect of substrate mass on the ejection yield have shown that the yield of an organic overlayer from a lighter carbon substrate is much less than that from a heavier metal substrate.<sup>33</sup> The 8 keV primary ions have kinetic energies that are orders of magnitude larger than the binding energy of any of the particles constituting C<sub>6</sub>H<sub>6</sub> molecules. As a result, the initial interaction of the primary projectile with the C<sub>6</sub>H<sub>6</sub> solid can be described by binary collisions with individual atoms rather than entire molecules. Using a simple binary collision approximation, it is easy to show that the lighter C atoms are far less effective at redirecting the momentum of the incident primary ion as compared to silver atoms. Fragmentation is also an issue for this situation.<sup>34,35</sup> With the increase in surface density of C<sub>6</sub>H<sub>6</sub> molecules, direct collisions with the incoming projectiles become more probable which lead to extensive bond breaking. All these effects reduce the overall yield of ejected intact molecules, as observed.

The effect of the change in molecular environment is also manifested in the kinetic energies of the ejected particles. The TOF distributions of neutral C<sub>6</sub>H<sub>6</sub> molecules obtained after 8 keV Ar<sup>+</sup> ion bombardment of C<sub>6</sub>H<sub>6</sub>/Ag{111} are shown in Figures 3 and 4. The distributions have strikingly different shapes depending on the C<sub>6</sub>H<sub>6</sub> exposure. As shown in Figure 3, at 1 langmuir exposure, only a component at short TOF (peak A) is present. At all exposures below 1 langmuir the TOF distributions are nearly identical, and for exposures above 1 langmuir the distribution begins to shift to longer TOF (inset,

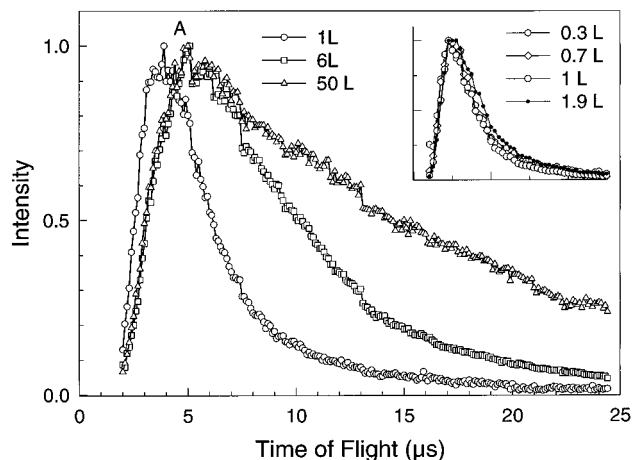


**Figure 3.** Time-of-flight distributions of neutral C<sub>6</sub>H<sub>6</sub> molecules for low exposures expressed in langmuirs (L). The distributions at extremely low exposures are shown in the inset.

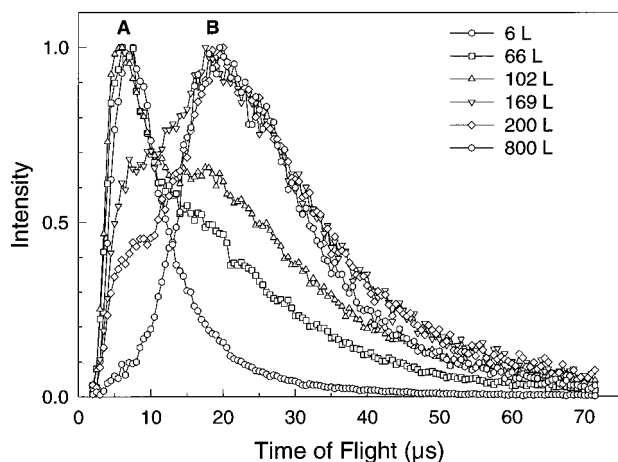


**Figure 4.** Time-of-flight distributions of neutral C<sub>6</sub>H<sub>6</sub> molecules for high exposures expressed in langmuirs (L). The high- and low-energy components are labeled A and B, respectively.

Figure 3). The successive shift in the peak A position to longer TOF continues up to 6 langmuirs exposure.

As shown in Figure 4, the TOF distribution for layers formed above 6 langmuirs exposure takes on a very different character than that seen below 6 langmuirs. Further increase in exposure after 6 langmuirs does not influence the position of peak A but rather results in an increase in signal intensity at long TOF (peak B). The intensity of peak A drops, and peak B begins to dominate the TOF distribution. At an exposure of 800 langmuirs only peak B is present. The mass spectrum of the species ejected at this exposure shows only peaks corresponding to the overlayer molecules. No Ag or Ag<sub>2</sub> signal is present, indicating that at 800 langmuirs exposure the thick overlayer prevents ejection of any substrate particles. Peak B can therefore be associated with the multilayer ice film. At intermediate exposures, both peaks are visible, suggesting that at least two different mechanisms are involved in the ejection process. These processes will be discussed separately for the low- and high-coverage regimes.

**Low Coverage.** The kinetic energy distributions of Ag<sub>2</sub> and C<sub>6</sub>H<sub>6</sub> molecules comprising peak A for low exposures are shown in Figure 5. When the C<sub>6</sub>H<sub>6</sub> distributions are fit to the Maxwell-Boltzmann equation, the resulting effective temperature is close to 11 000 K for 1 langmuir exposure and 5400 K for 6 langmuirs exposure. Since these values are unphysically high for a molecule such as C<sub>6</sub>H<sub>6</sub>, we presume that a thermal

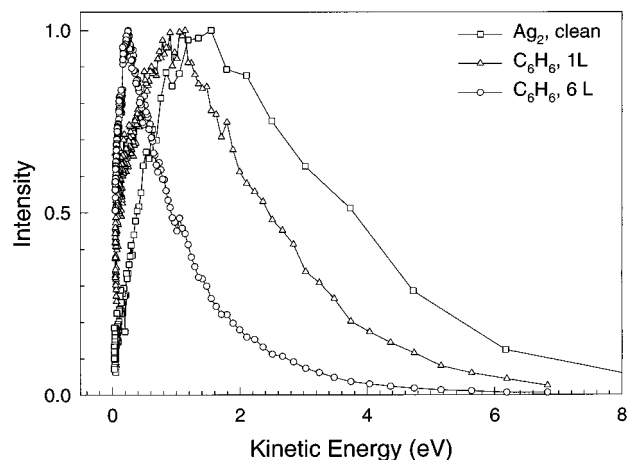


**Figure 5.** Kinetic energy distributions of Ag<sub>2</sub> emitted from a clean surface (□) and C<sub>6</sub>H<sub>6</sub> molecules comprising peak A, at 1 langmuir exposure (△) and 6 langmuirs exposure (○).

mechanism is inappropriate for these cases. However, as we will show for higher C<sub>6</sub>H<sub>6</sub> exposures (800 langmuirs), the fit temperature is close to 500 K, suggesting that a thermal mechanism is feasible for that case.

It is interesting to note that the kinetic energy distributions of C<sub>6</sub>H<sub>6</sub> at 1 langmuir and Ag<sub>2</sub> are quite similar. The C<sub>6</sub>H<sub>6</sub> and Ag<sub>2</sub> molecules eject with kinetic energies that are of the same order with their peak kinetic energies being 1 and 1.8 eV, respectively. According to our earlier calculations, 1 langmuir exposure corresponds to ~0.2 monolayer coverage. In this coverage regime, the molecules are far apart, and direct interaction between the C<sub>6</sub>H<sub>6</sub> molecules and the primary projectile is improbable. The ejection of C<sub>6</sub>H<sub>6</sub> molecules is therefore due to collisions between ejecting silver particles and the overlayer molecules. The ejection of molecules by a momentum-transfer process should depend on the projectile mass. We were unable to see any C<sub>6</sub>H<sub>6</sub> signal after 8 keV H<sub>2</sub><sup>+</sup> ion bombardment. This is because for simple binary collisions Ar<sup>+</sup> ions impart 10 times more energy to Ag than do H<sub>2</sub><sup>+</sup> ions. As a result, significant sputtering of silver particles and consequently C<sub>6</sub>H<sub>6</sub> molecules is much less probable with the lighter H<sub>2</sub><sup>+</sup> projectiles. The fact that no C<sub>6</sub>H<sub>6</sub> signal is observed with H<sub>2</sub><sup>+</sup> further confirms that a ballistic process is responsible for the ejection of C<sub>6</sub>H<sub>6</sub> molecules.

Of note is that such a comparison of the ejection of C<sub>6</sub>H<sub>6</sub> with Ag<sub>2</sub> brings additional questions of how dimers form and eject from the surface. Comparison with Ag distributions would undoubtedly have been more reasonable, but it is not possible due to experimental limitations. Detection of Ag by nonresonant ionization is not appropriate because the Ag signal contains contributions from fragmenting Ag<sub>2</sub>. Detection of Ag would therefore require a two-color resonant ionization scheme which could not be obtained with our laser system. No experimental data on sputtering of single-crystal Ag are presented in the literature. The only published measurements were performed on polycrystalline silver.<sup>36</sup> These measurements show that the kinetic energy distribution of Ag<sub>2</sub> is narrower than that of Ag atoms even though the peaks in the two distributions are comparable. Also, the yield measurements show that Ag<sub>2</sub> comprises a small fraction (~7%) of all the emitted particles. Therefore, the collisions of the sputtered Ag atoms will be the primary channel leading to C<sub>6</sub>H<sub>6</sub> ejection. This conclusion is further supported by molecular dynamics simulation results of ion bombardment of a (3 × 3) overlayer of C<sub>6</sub>H<sub>6</sub> on Ag{111}. The simulations show that the energy distributions of the ejected

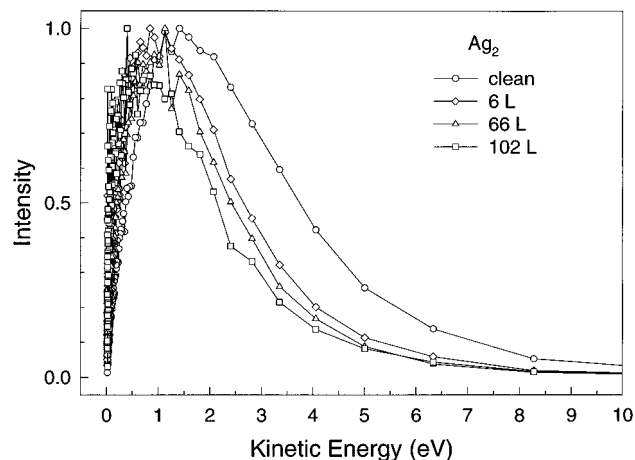


**Figure 6.** Kinetic energy distributions of  $\text{Ag}_2$  for various  $\text{C}_6\text{H}_6$  exposures.

$\text{C}_6\text{H}_6$  are comparable to that of  $\text{Ag}$ ,<sup>37</sup> and a majority of  $\text{C}_6\text{H}_6$  ejection is stimulated by collisions with these particles.

As the exposure is increased above 1 langmuir, the peak position in the kinetic energy distribution of  $\text{C}_6\text{H}_6$  molecules successively decreases from 1 to 0.25 eV at 6 langmuirs. This direct dependence of the kinetic energy distribution on  $\text{C}_6\text{H}_6$  coverage shows that, above  $\sim 0.2$  monolayer coverage, the intermolecular interactions begin to play an important role in the ejection of molecules. Below  $\sim 0.2$  monolayer coverage, the molecules are too far apart to interact with each other. Above  $\sim 0.2$  monolayer the intermolecular collisions become significant enough to lower the kinetic energy of the molecules. These collisions also clearly result in energy transfer to the internal modes of the molecules, which further reduces their average kinetic energy.

The kinetic energy distributions of  $\text{Ag}_2$  for various  $\text{C}_6\text{H}_6$  coverage are shown in Figure 6. As the overlayer coverage increases, the kinetic energy distributions shift toward lower energies. It is interesting to note that the molecular overlayer reduces the ejection of higher energy particles more than the lower energy ones. The loss in kinetic energy of the  $\text{Ag}_2$  particles is due to multiple collisions and scattering through the  $\text{C}_6\text{H}_6$  layer(s) during the ejection process.

Further insight into processes leading to ejection of  $\text{C}_6\text{H}_6$  at low coverage can be obtained from the angular distributions. These distributions are shown in Figure 7 for both  $\text{Ag}_2$  and  $\text{C}_6\text{H}_6$ . The angular distribution of  $\text{Ag}_2$  exhibits the same qualitative shape as that found for atoms ejected from  $\{111\}$  surfaces.<sup>38,39</sup> In general, this type of distribution has been explained via channeling and blocking of the ejecting species by other first-layer atoms. For example, the peak at a polar angle of  $30^\circ$  is thought to arise since there is a preferred takeoff path along three open crystallographic directions. These data are shown for the  $\langle 211 \rangle$  azimuth, which represents the strongest channeling direction. The peak at  $0^\circ$  or normal emission is thought to arise in part from second-layer atoms directed upward by structural openings in the top layer. These mechanisms have been confirmed for a variety of metals including  $\text{Rh}\{111\}$ <sup>38</sup> and  $\text{Au}\{111\}$ .<sup>39</sup> The above explanation will continue to hold for  $\text{Ag}\{111\}$  since ejection from metal single crystals is mainly dependent upon the crystal structure.

The behavior of the  $\text{Ag}_2$  polar angle distributions changes markedly with  $\text{C}_6\text{H}_6$  coverage. At 0.3 langmuir exposure the peak at  $30^\circ$  has lower intensity, and at 6 langmuirs it is completely suppressed. This is because the ejecting metal species no longer view the channeling and blocking pathways

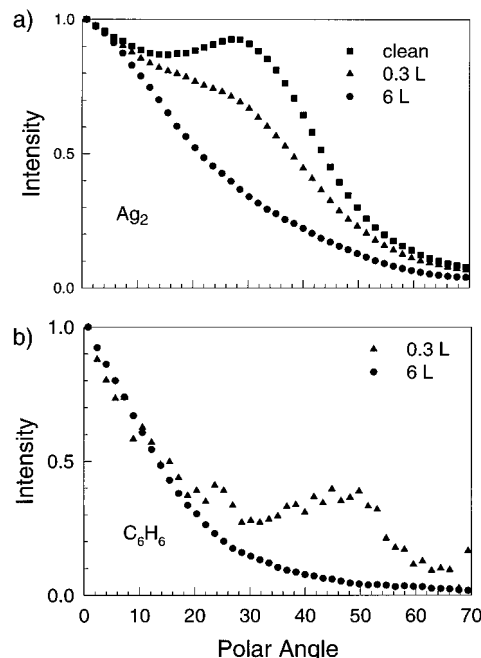


**Figure 7.** Polar angular distributions of (a)  $\text{Ag}_2$  and (b)  $\text{C}_6\text{H}_6$  for various  $\text{C}_6\text{H}_6$  exposures. The detection was performed along the  $\langle 211 \rangle$  azimuth.

present on the clean surface. The surface has basically lost its  $\{111\}$  character.

The  $\text{C}_6\text{H}_6$  polar angle distribution reveals a great deal about the ejection mechanism. At 0.3 langmuir exposure, there is a strong peak at  $48^\circ$  which is reminiscent of the underlying  $\text{Ag}$  substrate. These data imply that the  $\text{C}_6\text{H}_6$  molecules are ejected by direct collisions with substrate atoms and even retain some of the directional character associated with the collision cascade in the metal. The reason(s) behind the shift in the peak position from  $30^\circ$  on the clean surface to  $48^\circ$  on the 0.3 langmuir  $\text{C}_6\text{H}_6$  surface are not yet completely clear. A number of factors such as surface corrugation and surface binding energy can, however, influence the detailed shape of the distributions. Finally, note that at 6 langmuirs exposure all the anisotropy associated with the crystalline substrate has disappeared, suggesting that there are sufficient collisions with overlayer molecules to randomize the trajectories.

**High Coverage.** The kinetic energy distribution of the ejected  $\text{C}_6\text{H}_6$  molecules comprising peak B at 800 langmuirs exposure is shown in Figure 8. The molecules eject with extremely low kinetic energies close to 0.04 eV. Although, the data could be fit to a Maxwell–Boltzmann distribution using a temperature parameter of 518 K, this temperature is considerably different than the surface temperature of 117 K. Moreover, as shown in Figure 9, the TOF distributions are independent of surface temperature, although we could only test this effect over a limited range (117–134 K). These observations show that the  $\text{C}_6\text{H}_6$  molecules do not evaporate from areas that are in thermal equilibrium with the surface but are emitted with thermal energies that are higher than the macroscopic surface temperature. Local heating of the molecular solid, therefore, must stimulate emission of the weakly bound  $\text{C}_6\text{H}_6$  molecules.

Numerous phenomena might be responsible for such a behavior. The most obvious process is primary beam-induced evaporation. During ion bombardment a large fraction of the deposited energy goes to heat the sample.<sup>40</sup> For high ion beam fluxes in nonconducting solids, this energy is not effectively dissipated which leads to an increase in the surface temperature

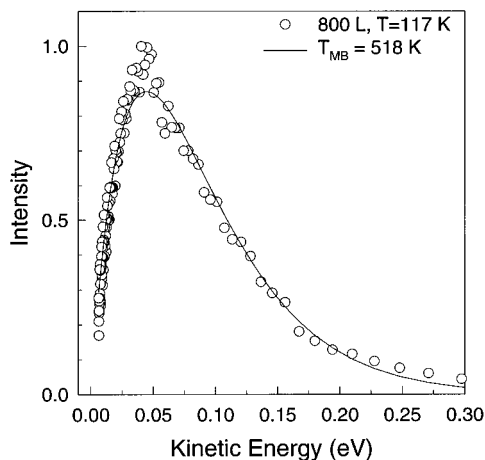


**Figure 8.** Kinetic energy distribution of C<sub>6</sub>H<sub>6</sub> at 800 langmuirs exposure comprising peak B (○). The solid line indicates a Maxwell–Boltzmann distribution with a fit temperature of 518 K.

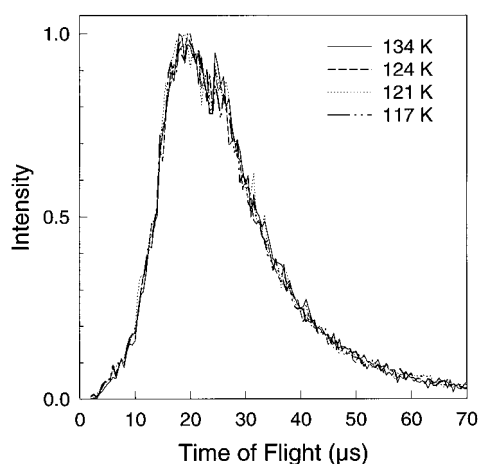


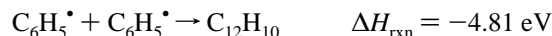
**Figure 9.** The time-of-flight distribution of C<sub>6</sub>H<sub>6</sub> at 800 langmuirs exposure for different surface temperatures.

and enhanced surface loss.<sup>41</sup> We exclude such a possibility, since our measurements were made at low ion dose where each impact can be treated as a separate event. Moreover, if beam heating occurs, one should expect the shape of the kinetic energy distribution to depend on the ion flux. No such dependence was observed in our measurements which show that the shape of the distribution does not depend on the ion pulse width (220–440 ns) or on the ion current (8–14 μA dc current).

Emission of molecules with low kinetic energies similar to those measured in our case have been observed in high dose electron, H<sub>2</sub><sup>+</sup>, He<sup>+</sup>, and Ar<sup>+</sup> stimulated desorption experiments on frozen methane (CH<sub>4</sub>) gases.<sup>17,42</sup> In these studies it was suggested that inelastic collisions lead to electronic excitation, ionization, or formation of radicals which subsequently react to form different species. These exothermic reactions could cause the formation of a region of higher temperature, and the species would emit with a near-Maxwellian distribution with fit temperatures higher than the surface temperature. In the present case, a similar process could be used to explain the low-energy emission and Maxwell–Boltzmann fit at temperatures higher than the surface temperature. Lighter projectiles should also induce emission of molecules by such processes. We were unable to detect any C<sub>6</sub>H<sub>6</sub> signal using 8 keV H<sub>2</sub><sup>+</sup> ion bombardment. Although ballistic ejection stimulated by H<sub>2</sub><sup>+</sup> projectiles is much less probable as compared to Ar<sup>+</sup> ions, the H<sub>2</sub><sup>+</sup> lighter projectiles are more efficient in depositing energy into the electronic system of the bombarded solid. The fact

that no C<sub>6</sub>H<sub>6</sub> signal is observed with H<sub>2</sub><sup>+</sup> shows at least that electronic excitation/ionization is directly not responsible for the low-energy emission.

The possibility that there are exothermic reactions of fragments formed by ballistic collisions, however, cannot be excluded. Ballistic fragmentation is much more probable for Ar<sup>+</sup> ions than it is for H<sub>2</sub><sup>+</sup> projectiles. The fragmentation of C<sub>6</sub>H<sub>6</sub> molecules near the primary ion impact zone yields highly reactive species such as H<sup>•</sup>, C<sub>6</sub>H<sub>5</sub><sup>•</sup>, and other ionic and molecular fragments.<sup>35,43</sup> These species may then react to form stable molecules. Possible scenarios are shown below.<sup>44</sup>



It has indeed been reported by Lancaster et al. that the secondary ion mass spectrum of frozen C<sub>6</sub>H<sub>6</sub> exhibits numerous peaks of clusters containing more than six C atoms.<sup>43</sup> Also, Zhou et al. have reported that phenyl (C<sub>6</sub>H<sub>5</sub><sup>•</sup>) and hydrogen (H<sup>•</sup>) radicals formed after interaction of high-dose, low-energy electrons with C<sub>6</sub>H<sub>6</sub>/Ag{111} react to form biphenyl (C<sub>12</sub>H<sub>10</sub>) and hydrogen molecules.<sup>45</sup> Kinetic studies of these reactions show that they occur in the femtosecond time scale.<sup>46</sup> Since these reactions are highly exothermic, they could cause the formation of a region of higher temperature. This would lead to the low-energy emission of C<sub>6</sub>H<sub>6</sub> molecules.

Finally, a momentum-transfer process can be responsible for the observed low-energy emission of C<sub>6</sub>H<sub>6</sub> molecules from multilayer samples. After primary ion impact a collision cascade develops in the molecular solid which involves multiple collisions between the molecules and fragments. This would lead to vibrational and rotational excitations of C<sub>6</sub>H<sub>6</sub> molecules. It is possible that the energy transferred to the internal modes of the molecules also leads to local heating of the surface. The emission of molecules with thermal energies higher than the macroscopic surface temperature can therefore be due to local heating caused by exothermic reactions and/or vibrational and rotational excitation of the C<sub>6</sub>H<sub>6</sub> molecules and fragments after ion bombardment.

## Conclusion

We have examined the kinetic energy, angular distributions, and relative yield of neutral C<sub>6</sub>H<sub>6</sub> molecules ejected from submonolayer to multilayer coverages of C<sub>6</sub>H<sub>6</sub> on Ag{111} by energetic ion bombardment. The results present a complex mechanistic picture suggesting that more than one mechanism is responsible for the ejection process, depending upon the chemical and physical properties of the C<sub>6</sub>H<sub>6</sub> overlayer. At low coverage, the data show that C<sub>6</sub>H<sub>6</sub> molecules are being ejected as a consequence of collisions with substrate particles. At intermediate coverage, the substrate particles continue to play a significant role in the ejection, but the energy distributions are influenced by intermolecular collisions between molecules. And finally, at the highest coverage representing a multilayer film, the behavior has more of a thermal nature. The thermal emission is proposed to occur due to exothermic chemical reaction of fragments formed in a molecular collision cascade of C<sub>6</sub>H<sub>6</sub> molecules. It is also possible that local heating occurs due to vibrational and rotational excitations of the molecules during the molecular collision cascade leading to thermal emission.

It is interesting that these results are quite different from those obtained for other molecules we have examined that have been adsorbed on metal surfaces. For phenethanethiol on gold, for example, we found that while a minor ejection occurs due to collisions from the Au atoms, most molecules desorb with thermal kinetic energies. The velocity distributions follow Maxwellian behavior with a temperature that closely track the substrate temperature.<sup>47</sup> For solid organic materials such as tryptophan though most molecules eject due to a ballistic process, emission of molecules for long times after ion impact is observed.<sup>48</sup> These data suggest that long-lived excited states may be involved in the desorption event. At this stage, then, the events that occur due to high-energy collisions cover a wide range of chemical and physical phenomena. It will be of future interest to see whether these phenomena can be categorized such that a generalized predictive formula may be utilized to decide how a particular molecule will behave. To achieve this end, we will need better molecular dynamics simulations to sort out the role of collisional processes, and we will need more experimental data on well-defined molecular systems with varied chemical properties.

**Acknowledgment.** The financial support of the National Science Foundation, the National Institute of Health, the Office of Naval Research, and the Polish Committee for Scientific Research and Maria Skłodowska-Curie Fund is gratefully acknowledged. The authors would also like to thank B. J. Garrison and R. Pedrys for helpful discussions.

## References and Notes

- (1) *Practical Surface Analysis*; Briggs, D., Seah, M. P., Eds.; Wiley: New York, 1992; Vol. 2.
- (2) *Secondary Ion Mass Spectrometry*; Vickerman, J. C., Brown, A., Reed, N. M., Eds.; Oxford University Press: New York, 1989.
- (3) Winograd, N. *Anal. Chem.* **1993**, *65*, 622A.
- (4) Benninghoven, A.; Hagenhoff, B.; Niehius, E. *Anal. Chem.* **1993**, *65*, 630A.
- (5) Pachuta, S. J.; Cooks, R. G. *Chem. Rev.* **1987**, *87*, 647 and references therein.
- (6) Ens, W. *Ken. Dan. Vid. Selsk. Mater. Fys. Medd.* **1992**, *43*, 155 and references therein.
- (7) Reimann, C. T. *Ken. Dan. Vid. Selsk. Mater. Fys. Medd.* **1992**, *43*, 351 and references therein.
- (8) King, B. V.; Tsong, I. S. T.; Lin, S. H. *Int. J. Mass Spectrom. Ion Processes* **1987**, *78*, 341.
- (9) Falcone, G.; Sroubek, Z.; Sindona, G.; Uccella, N. *Int. J. Mass Spectrom. Ion Processes* **1988**, *83*, 223.
- (10) Galera, R.; Blais, J. C.; Bolbach, G. *Int. J. Mass Spectrom. Ion Processes* **1991**, *107*, 531.
- (11) Urbassek, H. M. *Nucl. Instrum. Methods Phys. Res.* **1987**, *B18*, 587.
- (12) Haring, R. A.; Roosendaal, H. E.; Zalm, P. C. *Nucl. Instrum. Method Phys. Res.* **1987**, *B28*, 205.
- (13) Hoogerbrugge, R.; Kistemaker, P. G. *Nucl. Instrum. Methods Phys. Res.* **1987**, *B18*, 600.
- (14) Haring, R. A.; Pedrys, R.; Oostra, D. J.; Haring, A.; de Vries, A. E. *Nucl. Instrum. Methods Phys. Res.* **1984**, *B5*, 483.
- (15) Urbassek, H. M.; Michl, J. *Nucl. Instrum. Methods Phys. Res.* **1987**, *B22*, 400.
- (16) Kelly, R. *Nucl. Instrum. Methods Phys. Res.* **1990**, *B46*, 441.
- (17) Pedrys, R.; Oostra, D. J.; Haring, R. A.; Calcagno, L.; Haring, A.; de Vries, A. E. *Nucl. Instrum. Methods Phys. Res.* **1986**, *B17*, 15.
- (18) Haring, R. A.; Pedrys, R.; Oostra, D. J.; Haring, A.; de Vries, A. E. *Nucl. Instrum. Methods Phys. Res.* **1984**, *B5*, 476.
- (19) Thompson, M. W. *Philos. Mag.* **1968**, *18*, 377.
- (20) Menzel, D. *Nucl. Instrum. Methods Phys. Res.* **1995**, *B101*, 1 and references therein.
- (21) Pedrys, R.; Haring, R. A.; Haring, A.; Saris, F. W.; de Vries, A. E. *Phys. Lett.* **1981**, *82A*, 371.
- (22) Pedrys, R.; Haring, R. A.; Haring, A.; de Vries, A. E. *Nucl. Instrum. Methods Phys. Res.* **1984**, *B2*, 573.
- (23) Chatterjee, R.; Postawa, Z.; Garrison, B. J.; Winograd, N., to be published.
- (24) Sigmund, P. *Phys. Rev.* **1969**, *184*, 383.
- (25) De Vries, A. E. *Nucl. Instrum. Methods Phys. Res.* **1987**, *B27*, 173 and references therein.
- (26) Netzer, F. P. *Langmuir* **1991**, *7*, 2544.
- (27) Kobrin, P. H.; Schick, G. A.; Baxter, J. P.; Winograd, N. *Rev. Sci. Instrum.* **1986**, *57*, 1354.
- (28) Summers, R. L. *NASA Technical Note TN D-5285*, National Aeronautics and Space Administration: Washington, DC, 1969.
- (29) Dudde, R.; Frank, K. H.; Koch, E. E. *Surf. Sci.* **1990**, *225*, 267.
- (30) The 5 langmuirs exposure reported in ref 29 is also uncorrected for ion gauge sensitivity.
- (31) Mollers, R.; Schnieders, A.; Kortenbruck, G.; Benninghoven, A. *Second. Ion Mass Spectrom., SIMS 10* **1995**, 943.
- (32) O'Hanlon, J. F. *A User's Guide to Vacuum Technology*; John Wiley & Sons: New York, 1980; p 13.
- (33) Taylor, R. S.; Brummel, C. L.; Winograd, N.; Garrison, B. J.; Vickerman, J. C. *Chem. Phys. Lett.* **1995**, *233*, 575.
- (34) Moon, D. W.; Bleiler, R. J.; Karwacki, E. J.; Winograd, N. *J. Am. Chem. Soc.* **1983**, *105*, 2916.
- (35) Karwacki, E. J.; Winograd, N. *Anal. Chem.* **1983**, *55*, 790.
- (36) Wucher, A.; Garrison, B. J. *Surf. Sci.* **1992**, *260*, 257 and references therein.
- (37) Chatterjee, R.; Garrison, B. J. *Radiat. Eff. Defects Solids* **1997**, *142*, 127.
- (38) Garrison, B. J.; Reimann, C. T.; Winograd, N.; Harrison, D. E., Jr. *Phys. Rev. B* **1987**, *36*, 3516.
- (39) Rosencrance, S. W.; Winograd, N.; Garrison, B. J.; Postawa, Z. *Phys. Rev. B* **1996**, *53*, 1.
- (40) Johnson, R. E.; Schou, J. *Ken. Dan. Vid. Selsk. Mater. Fys. Medd.* **1992**, *43*, 403 and references therein.
- (41) Sigmund, P.; Szymanski, M. *Appl. Phys.* **1984**, *A33*, 141.
- (42) Calcagno, L.; Oostra, D. J.; Pedrys, R.; Haring, A.; de Vries, A. E. *Nucl. Instrum. Methods Phys. Res.* **1986**, *B17*, 22.
- (43) Lancaster, G. M.; Honda, F.; Fukuda, Y.; Rabalais, J. W. *J. Am. Chem. Soc.* **1979**, *101*, 1951.
- (44)  $\Delta H_{\text{rxn}}$  was calculated using the following parameters:  $\Delta H_f^\circ(\text{C}_6\text{H}_6) = 19.8$  kcal/mol,  $\Delta H_f^\circ(\text{C}_{12}\text{H}_{10}) = 43.52$  kcal/mol (ref 48);  $\Delta H_f^\circ(\text{C}_6\text{H}_5^+) = 77.2$  kcal/mol,  $\Delta H_f^\circ(\text{H}^+) = 52$  kcal/mol (ref 47).
- (45) Zhou, X.-L.; Castro, M. E.; White, J. M. *Surf. Sci.* **1990**, *238*, 215.
- (46) Zhou, X.-L.; Schwaner, A. L.; White, J. M. *J. Am. Chem. Soc.* **1993**, *115*, 4309.
- (47) Riederer, D. E.; Chatterjee, R.; Rosencrance, S. W.; Postawa, Z.; Dunbar, T. D.; Allara, D. L.; Winograd, N. *J. Am. Chem. Soc.* **1997**, *119*, 8089.
- (48) Riederer, D. E.; Chatterjee, R.; Winograd, N.; Postawa, Z. *RIS'96* **1996**, 371.
- (49) *CRC Handbook of Chemistry & Physics*, 66th ed.; CRC Press: Boca Raton, FL, 1986.
- (50) *The Chemical Thermodynamics of Organic Compounds*; Stull, D. R., Westrum, E. F., Jr., Sinke, G. C., Eds.; Robert E. Krieger Publishing Co.: Malabar, FL, 1987.